UC San Diego
UC San Diego Previously Published Works

Title
Structural basis for GPCR-independent activation of heterotrimeric Gi proteins

Authors
Kalogriopoulos, Nicholas A
Rees, Steven D
Ngo, Tony
et al.

Peer reviewed

Structural basis for GPCR-independent activation of heterotrimeric Gi proteins

Nicholas A. Kalogriopoulos[a,1], Steven D. Rees[b,1], Tony Ngo[b], Noah J. Kopcho[b,c], Andrey V. Ilatovskiy[b], Nina Sun[a], Elizabeth A. Komives[c], Geoffrey Chang[b,2], Pradipta Ghosh[a,d,e,2], and Irina Kufareva[b,2]

[a]Department of Medicine, University of California San Diego, La Jolla, CA 92093; [b]Skaggs School of Pharmacy and Pharmaceutical Sciences, University of California San Diego, La Jolla, CA 92093; [c]Department of Chemistry and Biochemistry, University of California San Diego, La Jolla, CA 92093; [d]Moores Cancer Center, University of California San Diego, La Jolla, CA 92037; and [e]Department of Cellular and Molecular Medicine, University of California San Diego, La Jolla, CA 92093

Heterotrimeric G proteins are key molecular switches that control cell behavior. The canonical activation of G proteins by agonist-occupied G protein-coupled receptors (GPCRs) has recently been elucidated from the structural perspective. In contrast, the structural basis for GPCR-independent G protein activation by a novel family of guanine-nucleotide exchange modulators (GEMs) remains unknown. Here, we present a 2.0-Å crystal structure of Gαi in complex with the GEM motif of GIV/Girdin. Nucleotide exchange assays, molecular dynamics simulations, and hydrogen–deuterium exchange experiments demonstrate that GEM binding to the conformational switch II causes structural changes that allosterically propagate to the hydrophobic core of the Gαi GTPase domain. Rearrangement of the hydrophobic core appears to be a common mechanism by which GPCRs and GEMs activate G proteins, although with different efficiency. Atomic-level insights presented here will aid structure-based efforts to selectively target the noncanonical G protein activation.

guanine-nucleotide exchange modulator (GEM) | GIV/Girdin | X-ray crystallography | hydrogen–deuterium exchange | molecular dynamics

H eterotrimeric G proteins act as molecular switches that gate the flow of information from extracellular cues to intracellular effectors that control cell behavior (1, 2). Canonically, heterotrimeric G protein signaling is initiated at the plasma membrane where agonist-bound G protein-coupled receptors (GPCRs) trigger dissociation of guanosine diphosphate (GDP) from Gαβγ trimers and release of Gβγ subunits; in other words, GPCRs serve as guanine nucleotide exchange factors (GEFs) (1). This signal is fine-tuned by GTPase-activating proteins (GAPs), guanine nucleotide dissociation inhibitors (GDIs), and other "accessory proteins" (3).

Among these accessory proteins, the recently delineated family of guanine-nucleotide exchange modulators, or GEMs (4, 5), stands out due to their ability to modulate heterotrimeric G proteins independently of GPCRs. GEMs are cytosolic proteins that uniquely act as GEFs for Gαi and as GDIs for Gαs, all using the same evolutionarily conserved GEM motif (6, 7). The motif was initially identified based on homology to the synthetic peptide KB752 that can bind and activate Gαi (8); however, the motif has since been found in several naturally occurring proteins (5). The ability of GEMs to activate Gαi in live cells downstream of diverse classes of receptors has been demonstrated by various approaches: Dissociation of Gβγ subunits from Gαi was shown using fluorescence and bioluminescence resonance energy transfer (FRET/BRET)-based reporters (9–11), Gαi activation by conformation-specific antibodies (12), and reduction in cellular cAMP by radioimmunoassay (12). These cited studies also demonstrated that the spatiotemporal patterns of GEM-mediated Gαi signaling are remarkably distinct from those triggered by GPCRs (4). Furthermore, published work has provided insight into GEM biology and demonstrated translational relevance of dysregulated GEM

signaling in disease (13), including cancer, organ fibrosis, and diabetes.

Because heterotrimeric G proteins are expressed in virtually all cell and tissue types, and are involved in most physiologic and pathologic processes, the molecular mechanism and structural determinants of G protein activation and action have been a top priority in the field, yielding over 70 publicly available structures in various conformations and complex compositions (*SI Appendix*, Table S1). The structural basis for GPCR-dependent G protein activation had challenged the field for decades but was revealed in the past 8 y by a series of landmark structural studies (14–18). These studies have demonstrated that one of the key mechanisms of G protein activation by GPCRs involves perturbation of the so-called hydrophobic core (19, 20) of the Gα GTPase domain, which is mediated by displacement of the C-terminal α5 helix and insertion of the GPCR's intracellular loop 2 (14–18).

Significance

Heterotrimeric G proteins are expressed in virtually all cell and tissue types and are involved in most physiologic and pathologic processes. As such, understanding the structural mechanism of G protein activation has been a top priority in the field, aimed at developing more effective pharmacological interventions. Recent breakthrough studies have elucidated the structural basis for G protein-coupled receptor (GPCR)-dependent G protein activation. In contrast, the structural basis of GPCR-independent G protein activation has remained elusive. The present study reveals the structural and dynamical basis for GPCR-independent Gαi activation by guanine-nucleotide exchange modulators (GEMs) and identifies key similarities and differences between GPCR-dependent and -independent activation mechanisms. These insights will be invaluable for efforts of selective pharmacological targeting of GEMs to treat GEM-driven diseases.

In contrast to these insights, the structural basis of GPCR-independent G protein activation has remained elusive (*SI Appendix*, Table S1). The present study reveals, at an atomic resolution, the structural and dynamical basis for Gαi activation by GEMs. These insights would be invaluable for efforts of selective pharmacological targeting of GEMs to treat GEM-driven diseases.

Results

Unique from GPCRs, GIV-GEM Binds and Stabilizes Switch II of Gαi. The first and most well-studied member of the GEM family is Gα-interacting vesicle-associated protein, or GIV/Girdin. GIV is a large, multidomain (*SI Appendix*, Fig. S1A) signal transducer that mediates G protein activation downstream a variety of cell-surface receptors to modulate diverse cellular processes (4, 21). GIV-dependent signaling has been implicated in a number of pathophysiologic conditions, including diabetes, fibrosis, and cancer (4).

Here, the 31-amino-acid GEM motif of GIV/Girdin (amino acids 1671–KTGSPGSEVVTLQQFLEESNKLTSVQIKSSS–1701) was cocrystallized with GDP-bound rat Gαi3 (henceforth Gαi•GDP) (*SI Appendix*, Table S2). In the crystallization construct, the flexible 25-amino-acid-long N-terminal helix of Gαi was deleted as done previously (8) and replaced by a His-tag followed by a short linker (SSGLVPRGSHM; *SI Appendix*, Fig. S1B, henceforth referred to as His-tag linker). The structure was determined to 2.0-Å resolution (Fig. 1 A and B and *SI Appendix*, Fig. S1).

The structure demonstrated that GIV-GEM binds at the typical effector binding interface: the hydrophobic pocket between Sw-II and the α3-helix of Gαi (Fig. 1 A and B). By forming a short antiparallel β-sheet with Sw-II residues Q204$^{G.s3h2.3}$–R208$^{G.H2.4}$ [superscript denotes Common Gα numbering scheme (22)], the peptide stabilizes Sw-II in a unique elevated conformation (Fig. 1 B–D). Key polar contacts at the interface include hydrogen bonding of GIV E1678 and E1688 to Gαi R208$^{G.H2.4}$, around which the peptide folds in a loop–helix conformation, and a hydrogen bond from GIV Q1683 with Gαi Q204$^{G.s3h2.3}$, a residue known for its role in GTP hydrolysis (23). The interface also features hydrophobic packing of GIV F1685 against W211$^{G.H2.7}$, I212$^{G.H2.8}$, F215$^{G.h2s4.1}$, and W258$^{G.H3.17}$ of Gαi, consistent with the established role of F1685 as the key interaction determinant (6). Residues L1682–N1690 of GIV form an α-helix that packs favorably across the α3-helix of Gαi (Fig. 1 B–D).

A number of Gαi residues engaged by GIV-GEM are shared by Gβγ and GoLoco GDIs (Fig. 1 D–G and *SI Appendix*, Fig. S2). For example, R208$^{G.H2.4}$ is important for RGS14, and K209$^{G.H2.5}$ is
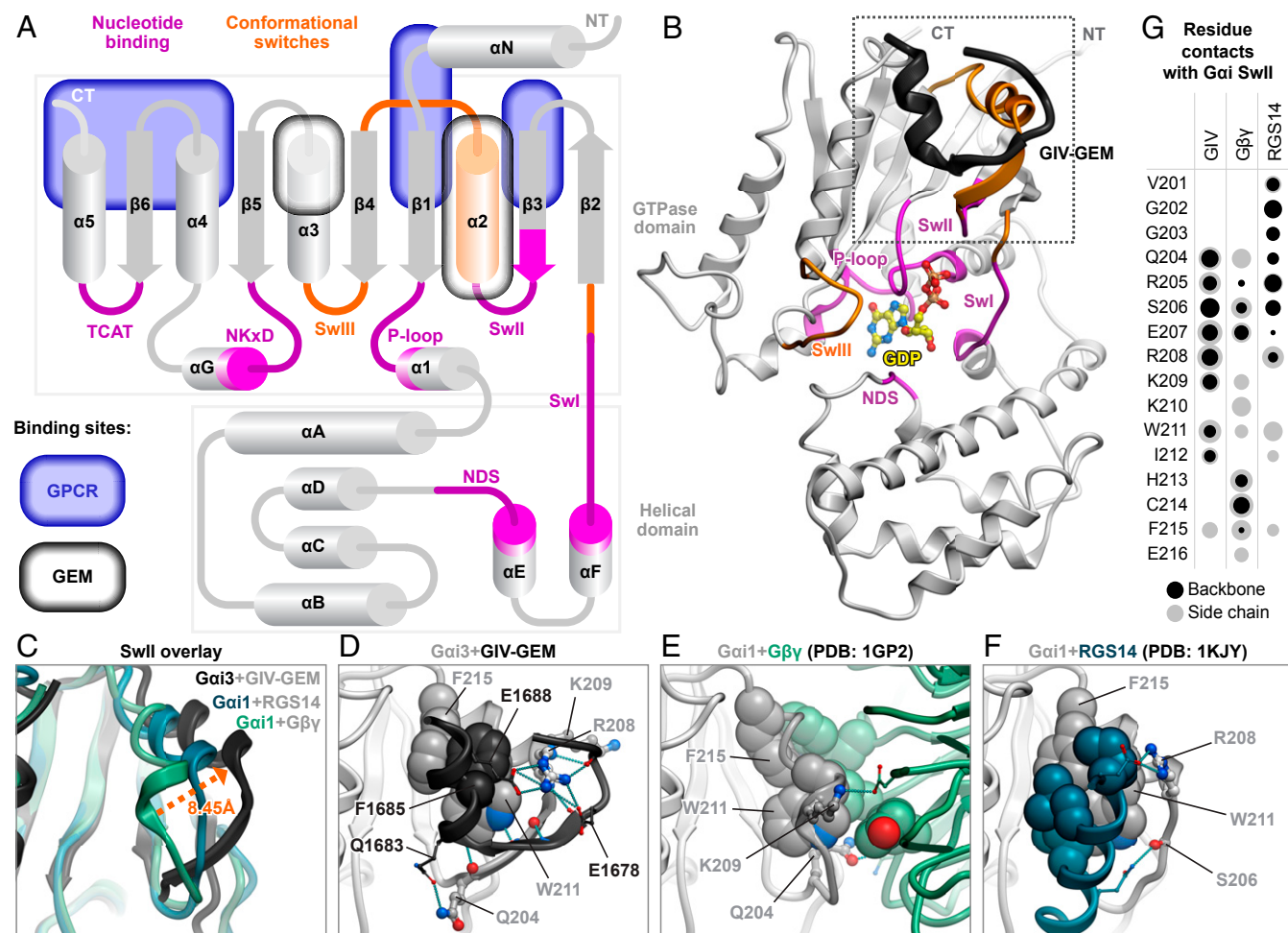
Fig. 1. GIV-GEM binds Sw-II of Gαi. (A) Topology of the Gαi protein with conformational switches and binding sites of key interactors marked. (B) Crystal structure of Gαi with GIV-GEM peptide bound at Switch (Sw)-II. (C) Overlay of Gαi Sw-II from Gβγ-bound, GDI-bound, and GIV-GEM–bound crystal structures. (D) A close-up view of the interaction interface between Gαi and GIV-GEM. (E and F) Close-up views of Gαi Sw-II bound to Gβγ [E, PDB ID code 1GP2 (36)] or GoLoco-motif GDI RGS14 [F, PDB ID code 1KJY (31)]. Key Sw-II residues shared by GIV and at least 1 of Gβγ or RGS14 are shown as spheres (aromatic/aliphatic) or sticks (polar). (G) Bubble plot displaying the strength and the nature of contacts that Gαi Sw-II residues make with GIV-GEM, Gβγ, or RGS14. The size of the dot is proportional to the strength of the contact (57); backbone and side-chains contacts are shown in black and gray, respectively.
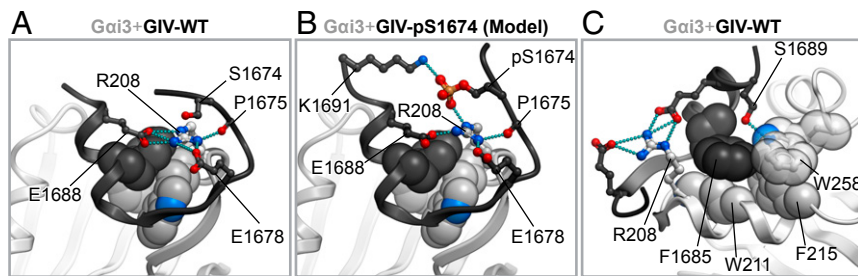
Fig. 2. Structural basis for phosphoregulation of GIV binding and activity toward Gαi. (*A*) Structure of WT GIV-GEM, highlighting unphosphorylated S1674 and the various contacts of R208$^{G.H2.4}$ of Gαi. (*B*) Model of (pS1674)GIV-GEM highlighting the formation of an additional direct contact with R208$^{G.H2.4}$. (*C*) Structure of WT GIV-GEM, highlighting a polar contact that unphosphorylated S1689 makes with W258$^{G.H3.17}$ of Gαi.

critical for Gβγ. These findings provide insight into the mutual exclusivity of GIV and Gβγ, or GIV and GoLoco GDI, binding to Gαi (6, 24). Although paralleling the phenomenon of Gβγ displacement by GPCRs, this mutual exclusivity has a different basis; in the case of GIV, it is not mediated by nucleotide exchange. Instead, the plausible mechanism of GIV–Gβγ competition is similar to that employed by GoLoco GDIs and involves GIV "capturing" the post-GTP hydrolysis Gαi molecules, thus preventing their reassociation with Gβγ.

The basis for the previously described phosphoregulation of GEM activity of GIV (25, 26) is evident from the structure and molecular modeling. A phosphate on the N-terminal S1674 of GIV-GEM is predicted to improve binding by creating an additional polar contact with Gαi R208$^{G.H2.4}$ (Fig. 2 *A* and *B*). By contrast, a phosphate on the C-terminal S1689 of GIV-GEM would disrupt a key hydrogen bond that this residue forms with W258$^{G.H3.17}$ of Gαi (Fig. 2*C*). These findings explain the opposing roles of the two phosphoevents: The former is known to enhance and the latter to abrogate the ability of GIV to bind and activate Gαi (25, 26).

Homology modeling of other GEM family members, Daple and NUCB1, suggested a conserved mode of binding with a few subtle differences that corroborate prior mutagenesis findings (27–29) (Fig. 3 *A–E*). Both Daple and NUCB1 appear to form a salt bridge with Gαi K248 (Fig. 3 *D* and *E*), which is not available to GIV due to a nonacidic residue in the position of Q1683 (Fig. 3*C*). However, GIV and Daple, but not NUCB1, form a hydrogen

bond with Gαi W258$^{G.H3.17}$, due to a Ser-to-Thr substitution in NUCB1 (Fig. 3 *C* and *D*). The presence of both hydrogen bonds in Daple explains its tolerance toward individual mutations of K248$^{G.H3.7}$ or W258$^{G.H3.17}$, whereas binding of GIV and NUCB1 to Gαi is lost exclusively upon mutations of W258$^{G.H3.17}$ or K248$^{G.H3.7}$, respectively (27–29). Interestingly, the GEM motif of NUCB1 maps onto one of the EF-hand motifs of this protein (30); modeling suggests not only full compatibility of the EF-hand topology with Gαi Sw-II binding but also structural mimicry between such binding and the canonical EF-hand–mediated molecular fold (Fig. 3*F*).

In our structure, the His-tag linker of each molecule binds to its symmetry neighbor, positioning the linker Arg and surrounding residues across the nucleotide cleft in a manner similar to GoLoco GDIs (31) (*SI Appendix*, Fig. S3 *A–C*). Removal of the His-tag linker or changing its position produced no crystals, suggesting that the linker trapped an otherwise transient and likely noncrystallizable GEF-induced conformation of Gαi·GDP. Although often overlooked, crystal packing against Sw-I is in fact quite prevalent in published Gαi crystal structures (2, 32). Here we sought to directly assess if the observed packing confounded any of the structural findings about GIV-GEM interface with Gαi. To this effect, we determined the structure of the His-tag linker-containing Gαi·GDP with KB752 (*SI Appendix*, Fig. S3 *A* and *E–G*) and compared it to a previously published complex without the His-tag linker (8) (Protein Data Bank [PDB] ID code 1Y3A). No discernible differences were noted in the Gαi–KB752 interface
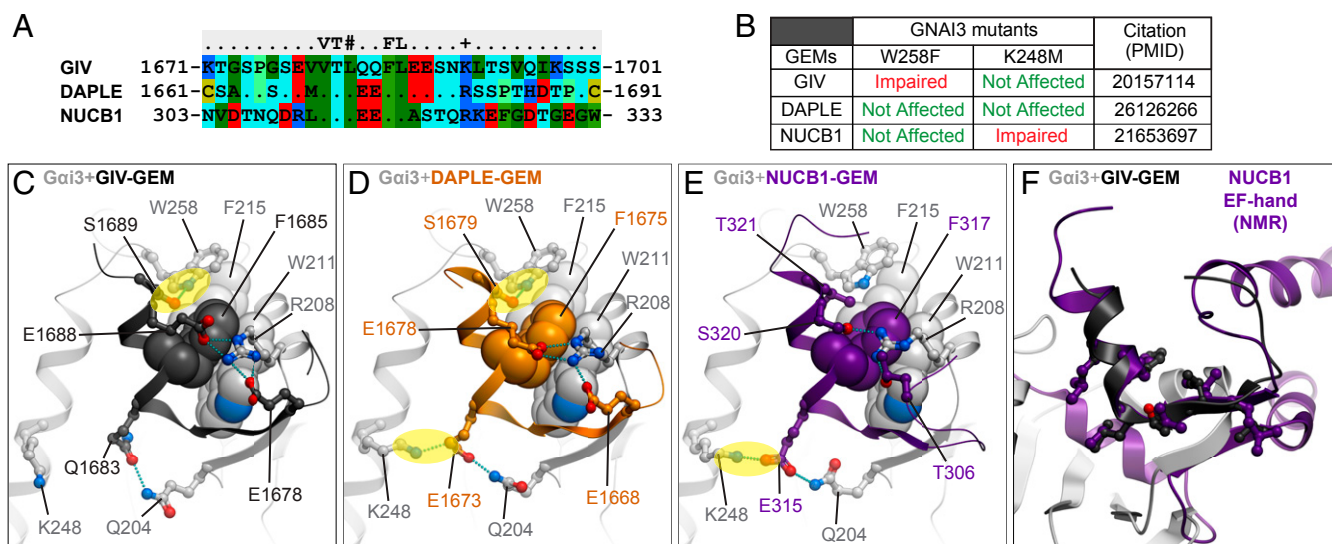
Fig. 3. Homology models of Gαi·GDP bound to the various members of the GEM family suggest a conserved mechanism of binding and action. (*A*) Sequence alignment of the GEM motifs within human GIV, Daple, and NUCB1 (Calnuc) sequences. (*B*) Table summarizing previous mutagenesis studies. (*C*) Crystal structure of GIV-GEM bound to Gαi. (*D* and *E*) Homology models of (*D*) Daple and (*E*) NUCB1 bound to Gαi created using the GIV-GEM–bound structure as template. Hydrogen bonds explaining the mutagenesis in *B* are highlighted. (*F*) Overlay of our GIV-GEM–bound Gαi structure with the EF-hand motif of NUCB1, previously determined by NMR (PDB ID code 1SNL).

(*SI Appendix*, Fig. S3 *F* and *G*), suggesting that the observed features at the Gαi–GIV-GEM interface are also representative of the native interactions. By contrast, pronounced differences were observed in the position of Gαi Sw-I, which is found in an inward-collapsed conformation in the linker-free structure of Gαi–KB752 complex (8) but is propped by the crystal neighbor's His-tag linker in an outward conformation in our linker-containing structure of the same complex (*SI Appendix*, Fig. S3G). Consequently, we use caution in our interpretation of Sw-I position in the Gαi-GIV-GEM structure, and henceforth validate all structural observations with orthogonal biochemical, biophysical, and computational methods.

GIV-GEM Binding Disfavors the High-GDP-Affinity Conformations of Gαi Sw-II and Q204[G.s3h2.3]. Upon binding, GIV-GEM accelerates the basal nucleotide exchange of monomeric Gαi (6). To understand the structural basis for this phenomenon, we compared the newly determined structure with all previously crystallized GDP-bound complexes of Gαi. The complexes were organized in order of decreasing GDP affinity, from GoLoco GDI-bound and Gβγ-bound (high GDP affinity), through GDP-only (basal affinity) to KB752- and GIV-bound (low GDP affinity). A clear trend emerged in the position of Sw-I and the molecular contacts of Q204[G.s3h2.3] in Sw-II. In high-GDP-affinity states, Q204[G.s3h2.3] appears to stabilize Sw-I in an outward position, away from the nucleotide-binding pocket (Fig. 4 *A* and *B*). By contrast, in the KB752-bound Gαi structures (ref. 8 and this work), Q204[G.s3h2.3] is displaced away from Sw-I; in the His-tag linker-free structure (8), this allows Sw-I to "collapse" toward the bound nucleotide

(Fig. 4*D*). GIV-GEM produces a similar but more exacerbated effect: It stabilizes an elevated conformation of Sw-II, hydrogen-bonds to Gαi Q204[G.s3h2.3] via Q1683, and pulls it ~11 Å away from Sw-I, leading to an even greater contraction of the GDP phosphate binding site that also involves a displacement of the β2-strand (Fig. 4 *E* and *F*). Despite this collapse, the N-terminal part of Sw-I is found in the outward position, due to the His-tag linker-mediated crystal packing (Fig. 4*E*).

These observations prompted us to probe the role of Gαi Q204[G.s3h2.3] in GIV-GEM–mediated GDP release. A Q204[G.s3h2.3]A mutant was generated and tested in a kinetic assay where GDP released from Gαi is replaced by MANT-GTPγS, a nonhydrolyzable fluorescent GTP analog (33, 34). Because GDP release is the rate-limiting step of nucleotide exchange, increases in MANT-GTPγS incorporation rate by Gαi reflect the acceleration of GDP release (35). Gαi(Q204[G.s3h2.3]A) fully retained its ability to bind GTP (*SI Appendix*, Fig. S4*A*). Compared with wild type (WT), Gαi(Q204[G.s3h2.3]A) displayed a small but consistent increase in the basal GDP exchange rate (1.28-fold; Fig. 4 *G* and *H*). However, the mutant was significantly more sensitive to activation by GIV-GEM (3.25-fold compared with 1.84-fold for WT Gαi; Fig. 4 *G* and *H*). These findings suggest that Q204[G.s3h2.3] indeed negatively regulates GDP release, likely by stabilizing Sw-I in the high-GDP-affinity state. Interestingly, the direct contact between GIV Q1683 and Gαi Q204[G.s3h2.3] appears unnecessary for accelerated nucleotide exchange because a GIV(Q1683A) mutant fully retained its GEF function (*SI Appendix*, Fig. S4 *B* and *C*).
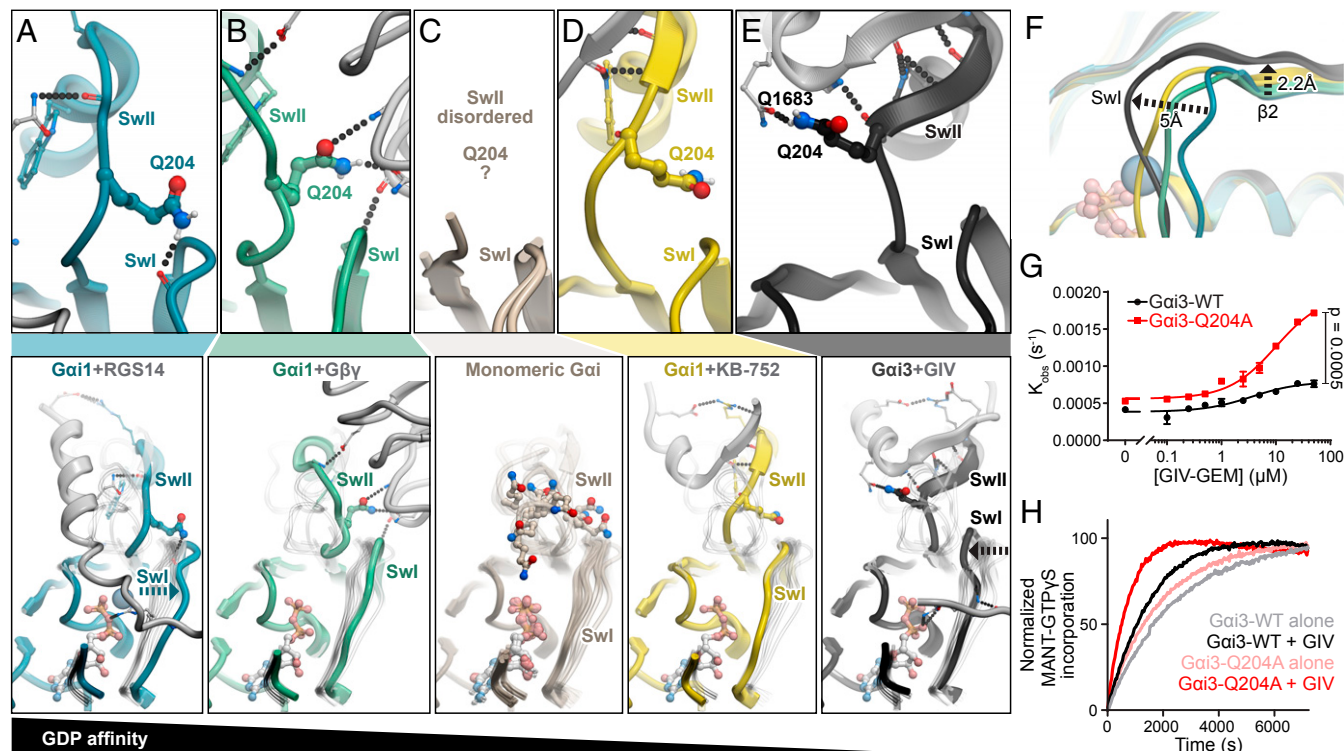
Fig. 4. GIV binding to Sw-II of Gαi disrupts GDP-stabilizing interactions between Sw-II and Sw-I and induces a low-GDP-affinity conformation of Gαi. (*A–E*) Comparison of Sw-I, Sw-II, and Q204 in various GDP-bound structures of Gαi, arranged from high (*Left*) to low (*Right*) GDP-affinity states. In the top part of *C*, the only two existing structures of GDP-bound monomeric WT Gαi are shown, PDB ID codes 1BOF and 1GDD, both with disordered Sw-II. (*F*) Overlay of structures shown in *A*, *B*, *D*, and *E*, highlighting differences in Sw-I and the β2-strand. (*G*) MANT-GTPγS incorporation into WT and Q204A[G.s3h2.3] Gαi proteins was assessed in the presence of varying concentrations of WT GIV-GEM peptide. Findings are displayed as a line graph showing observed rates (k_{obs}, s^{-1}) for nucleotide incorporation. Data shown are triplicates from a representative experiment; $n = 3$. (*H*) Same data as in *G* presented as a line graph showing average nucleotide incorporation over time in the presence or absence of 50 µM WT GIV-GEM peptide. Statistical significance between means was calculated using multiple comparisons in one-way nonparametric ANOVA.

Binding of GIV-GEM to Gαi Overcomes the Allosteric GDP-Stabilizing Role of Hydrophobic Residues in Sw-II. Besides Q204[G.s3h2.3], GIV-GEM directly engages the aromatic residues W211[G.H2.7] and F215[G.h2s4.1] in Sw-II of Gαi; these residues were previously proven critical for GIV-GEM binding (6). Structural comparisons suggest that each of these residues is stabilized by GIV-GEM in a different position compared with the high-GDP-affinity Gβγ- [PDB ID code 1GP2 (36)] or GoLoco-bound [PDB ID code 1KJY (31)] states (*SI Appendix*, Fig. S5). The rmsd of the W211[G.H2.7] side chain between the GIV-GEM–bound and GoLoco-bound structures is ~2.7 Å, and its rotamer states are completely different. The side chain of F215[G.h2s4.1] is also displaced ~6.4 Å in the GIV-GEM–bound structure compared with the heterotrimer structure. These findings suggest that the conformations of W211[G.H2.7] and F215[G.h2s4.1] in Gαi Sw-II may be important for regulating GDP affinity, and that the packing of these bulky hydrophobic residues against the β-barrel of the GTPase domain may stabilize GDP in the basal state (Fig. 5*A*). If so, binding of GIV-GEM to Sw-II may neutralize such GDP-stabilizing effects to stimulate GDP release. Corroborating this hypothesis, alanine mutants W211[G.H2.7]A or F215[G.h2s4.1]A retained the ability to bind GTP (*SI Appendix*, Fig. S6*A*) but resulted in substantial increases in the basal nucleotide exchange rate of Gαi in MANT-GTPγS incorporation assays (2.48- and 1.84-fold increases, respectively; Fig. 5 *B* and *C*). By contrast, mutation of V218[G.h2s4.4]A, a hydrophobic

residue on Sw-II that is not necessary for GIV-GEM binding, showed a small decrease in nucleotide exchange rate (Fig. 5 *B* and *C*). Consistent results were obtained in thermal stability assays where the two fast-exchanging Gαi mutants, W211[G.H2.7]A and F215[G.h2s4.1]A, displayed lower melting temperatures in both native and GDP-bound state compared with WT Gαi and Gαi(V218[G.h2s4.4]A) (*SI Appendix*, Fig. S6 *B* and *C*). These results support the idea that W211[G.H2.7] and F215[G.h2s4.1] on Sw-II contribute to stabilization of the bound GDP, an effect that is neutralized by GIV-GEM binding.

To understand the global allosteric changes in Gαi caused by the loss of bulky hydrophobic residues in Sw-II, we subjected WT and mutant Gαi to hydrogen–deuterium exchange mass spectrometry (HDX-MS), a sensitive technique that uses deuterium labeling of protein backbone amides (37) to probe conformational dynamics and mutation-induced allostery (38, 39) (*SI Appendix*, Table S3). The V218[G.h2s4.4]A mutant showed only slight decreases in deuterium uptake compared with WT Gαi, notably in the C-terminal end of the α3-helix through the α3-β5 loop (residues F250[G.H3.9]–S263[G.S5.1], 3.0% decrease) and the C-terminal end of the α5-helix (residues A338[G.H5.10]–N347[G.H5.19], 2.3% decrease) (Fig. 5*D* and *SI Appendix*, Fig. S7). By contrast, the fast-exchanging W211[G.H2.7]A mutant exhibited regions of higher deuterium uptake indicative of increased dynamics. The segment spanning Sw-I and the β2-strand (residues R176[H.HF.6]–F191[G.S2.8]) showed the highest
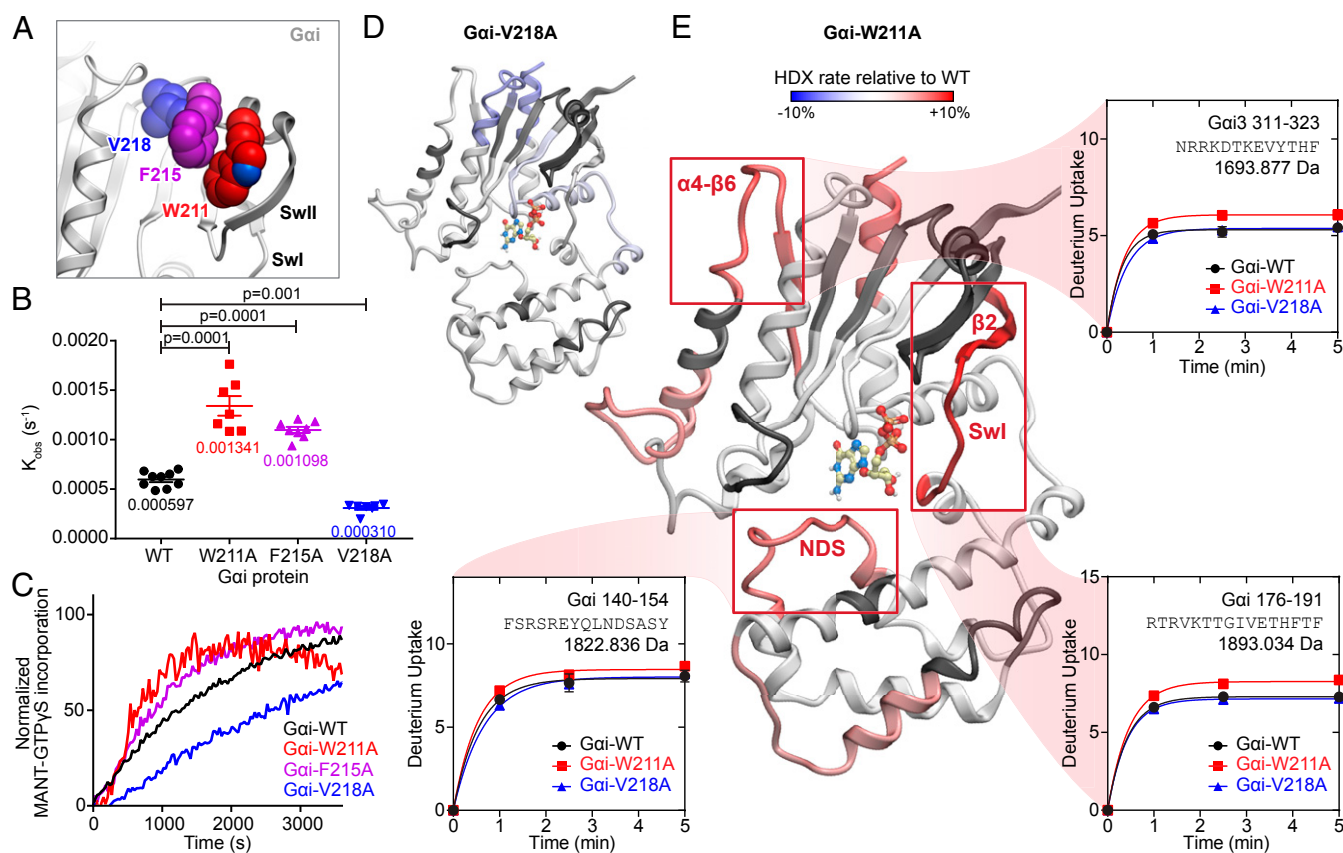
Fig. 5. Bulky hydrophobic residues in Sw-II of Gαi that are engaged by GIV stabilize GDP and influence the dynamics of Sw-I and the β2-strand. (*A*) Structure showing hydrophobic residues in Sw-II of Gαi that were subjected to mutagenesis. (*B* and *C*) MANT-GTPγS incorporation into WT, W211A[G.H2.7], F215A[G.h2s4.1], and V218A[G.h2s4.4] Gαi. Findings are displayed as a dot plot (*B*) showing the observed nucleotide incorporation rates (k_{obs}, s^{-1}) and as line graphs (*C*) showing average nucleotide incorporation over time. Data shown are from three independent experiments; $n = 9, 7, 8$, and 7 for WT, W211A[G.H2.7], F215A[G.h2s4.1], and V218A[G.h2s4.4], respectively. (*D* and *E*) Differences in relative deuterium uptake between V218A[G.h2s4.4] and WT Gαi (*D*) and between W211A[G.H2.7] and WT Gαi (*E*) at 5 min, as determined by triplicate HDX-MS assays. Blue and red coloring corresponds to −10% and +10% change, respectively; black indicates regions that were not mapped. Regions exhibiting increased uptake in the W211A[G.H2.7] mutant are highlighted and the corresponding deuterium uptake plots shown (SD error bars are within the symbols). Statistical significance between means was calculated using multiple comparisons in one-way nonparametric ANOVA.

increase in deuterium uptake in the W211$^{G.H2.7}$A mutant compared with the WT protein (7.2% increase; Fig. 5E and *SI Appendix*, Fig. S7). Other regions with moderately increased deuterium uptake in the mutant include the αA–αB loop and part of the αB helix (residues K92$^{H.hahb.1}$–L107$^{H.HB.9}$, 2.5% increase), the αD–αE loop including the so-called NDS motif (residues F140$^{H.HD.7}$–Y154$^{H.HE.4}$, 4.2% increase), part of the αG–α4 loop and α4-helix (residues I285$^{G.HG.17}$–A301$^{G.H4.6}$, 3.3% increase), the C-terminal end of the α4-helix through the β6-strand (residues N311$^{G.h4s6.2}$–F323$^{G.S6.5}$ and E308$^{G.H4.26}$–F323$^{G.S6.5}$, 5.6% increase), and the C-terminal end of the α5-helix (residues A338$^{G.H5.10}$–N347$^{G.H5.19}$, 3.0% increase) (Fig. 5E and *SI Appendix*,
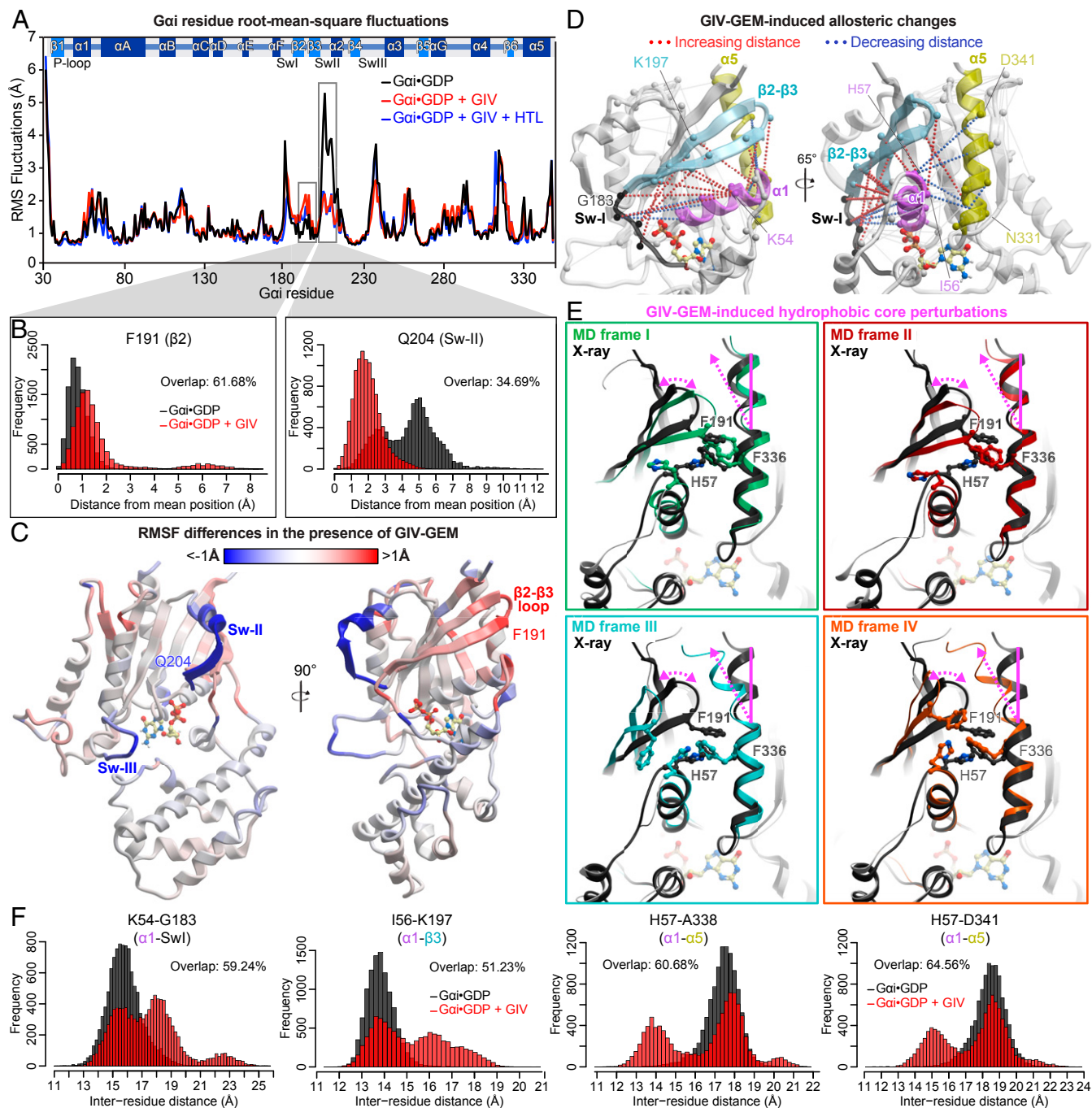
Fig. 6. Binding of GIV-GEM overcomes the GDP-stabilizing role of Sw-II and releases conformational constraints on Sw-I, β2–β3 strands, and the hydrophobic core of the GTPase domain. (A) Root mean square fluctuations (RMSF, angstroms) of Gαi residues as determined by molecular dynamics simulations under the three specified conditions. (B) Representative histograms showing the distribution, across all simulation frames, of residue rmsd in relation to the mean position of the same residue (F191 in the left and Q204 in the right). (C) Residue RMSF differences between the GIV-GEM–bound Gαi•GDP and Gαi•GDP alone mapped onto the structure of Gαi. (D) Intramolecular distances where the most significant changes between the two simulation conditions (as in C), as determined by PCA, are shown as dotted lines; significant distances beyond the hydrophobic core are colored silver. (E) Representative frames from the MD simulations highlighting the conformational changes allosterically induced by GIV-GEM and perturbation of key interactions in the hydrophobic core of Gαi. (F) Distribution of interresidue distances for the indicated residue pairs throughout the molecular dynamics simulations.

Fig. S7). Although it is impossible to state whether these changes are a trigger or a consequence of GDP release, the findings are consistent with the role of W211[G.H2.7] on Sw-II as an allosteric stabilizer of Sw-I and the β2-strand of Gαi, and thus of the overall high-GDP-affinity state of the protein. Of note, the relatively small magnitude of the observed changes in deuteration was not unexpected, as these changes were determined in comparison with monomeric WT GDP-bound Gαi, whose basal state is very dynamic when it is not stabilized by Gβγ.

Interestingly, at an earlier 1-min time point, four regions within the W211[G.H2.7]A mutant (residues T120[H.hbhc.15]–C139[H.HD.6], C224[G.s4.5]–D231[G.s4h3.5], F267[G.S5.5]–F274[G.HG.4], and V335[G.H5.7]–D341[G.H5.13]) showed reduced deuterium uptake compared with WT (*SI Appendix*, Fig. S7). In other words, for these regions the localized motions which gradually exposed amide protons to deuterium exchange appeared partially slowed by the W211[G.H2.7]A mutation, with uptake into the W211[G.H2.7]A mutant reaching that of WT Gαi only by 5 min of incubation with deuterium. These segments stand out in contrast to the enhanced dynamics observed for Sw-I, β2-strand, α4–β6 loop, and NDS loop, where greater deuterium uptake was observed throughout all measured time points. The reason for these differences may be entropic compensation—a known phenomenon (40) whereby reduced dynamics of some regions in the protein structure compensates for an enhancement in others.

Molecular Dynamics Simulations Reveal GIV-Induced Rearrangements in the Hydrophobic Core of Gαi. To gain further insights into the allosteric regulation of Gαi and the mechanism by which GIV-GEM accelerates GDP release, we carried out molecular dynamics (MD) simulations. Using the crystallized conformation of Gαi·GDP as a starting point, 350 ns of protein dynamics were simulated in triplicates for the GDP-only and GIV-GEM–bound states (1,050 ns total for each state) and 3 × 200 ns were simulated in the GIV-GEM+His-tag linker–bound state. A root mean square fluctuation (RMSF) analysis of the centers of mass of Gαi residues demonstrates that Sw-II is highly dynamic in the GDP-only simulation (Fig. 6 *A* and *B*), in agreement with its invariably disordered state in WT Gαi·GDP crystal structures (32, 41, 42) (Fig. 4*C*). Binding of GIV-GEM to Gαi Sw-II increased its rigidity as expected, but it also unexpectedly stabilized Sw-III that has no direct contact with the peptide (Fig. 6 *A–C*). The most striking increase in dynamics was observed in the C-terminal region of Sw-I and the β2-β3 strands (Fig. 6 *B* and *C*), which normally pack against the α1- and α5-helices of Gαi to form the hydrophobic core (20) of the GTPase domain. When simulations were run in the presence of the His-tag linker, the dynamics of Sw-II was unchanged with respect to the GIV-bound state, the high mobility of Sw-III was restored to the GDP-only level, and the GIV-induced increase in Sw-I and β2–β3 strand dynamics was partially negated, in agreement with a potential role of the His-tag linker in stabilizing GIV-GEM–bound Gαi and facilitating its crystallization (*SI Appendix*, Fig. S8*A*). These data support the idea that binding of GIV-GEM to Sw-II allosterically perturbs Sw-I and the β2-strand; it also suggests that the perturbation is further propagated to the hydrophobic core of the GTPase domain of Gαi.

To pinpoint the dominant allosteric changes in Gαi induced by GIV-GEM, we projected the pairwise Gαi residue (center of mass) distances onto a lower-dimension space via principal component analysis (PCA; *SI Appendix*, Fig. S8*B* and Table S4). Sw-II was excluded from the PCA to selectively detect allosteric changes rather than direct consequences of GIV-GEM binding. In the first principal component, the largest contributions were from the residue distances within the hydrophobic core of the GTPase domain that changed consistently and substantially upon GIV-GEM binding: Those from the β2–β3 strands to helix α1 systematically increased, and those from α1 to α5 systematically

decreased (Fig. 6 *D–F* and *SI Appendix*, Fig. S8*C*). Analysis of representative Gαi conformations from different areas in the PC space demonstrates that GIV-GEM binding allosterically induces an outward motion of the β2–β3 loop with a concomitant tilting of the C-terminal part of the α5 helix toward the β2–β3 strands, drastically perturbing the intramolecular packing in the hydrophobic core (Fig. 6*E*). Of note, the tilt in α5 conformation was found to correlate with GDP release in other studies as well (43). In addition, GIV-GEM binding resulted in a distance increase between GDP and R178[G.hfs2.2] (a residue known to stabilize GDP) and a concomitant decrease in distance between the GDP and the αF-helix (preceding Sw-I) (*SI Appendix*, Fig. S8 *D–F*), indicative of inward collapse of Sw-I as predicted (Fig. 4). Many of the Gαi residues highlighted by this analysis were retrospectively found to play important roles in GDP binding (44).

GDP dissociation did not occur over the course of our 3 × 350-ns simulations with GIV-GEM, consistent with the reported high affinity of GDP to Gαi and its ability to stay bound through much longer simulations (total 42-μs simulation for Gαi-GDP only) unless the protein conformation is substantially perturbed (18).

Discussion

The present work provides an atomic-level structure of a naturally occurring GEM bound to Gαi. The structure provides mechanistic insights into key aspects of GEM biology, including the mutual exclusivity of GEM binding with Gβγ (which promotes Gβγ signaling) and GoLoco-containing proteins (which antagonizes the GDI action of such proteins) (6, 24). Furthermore, the structure explains the basis for phosphoregulation of GIV-GEM.

This study also elucidates the mechanism by which GEMs accelerate GDP release from Gαi. MD simulations, HDX-MS, and nucleotide exchange experiments reveal a previously unknown role of Gαi Sw-II in nucleotide affinity. Stabilization of the elevated Sw-II conformation by GIV-GEM releases conformational constraints on Sw-I and β2–β3 strands of Gαi, allowing for inward collapse of the former and higher mobility of the latter. This perturbation propagates to the hydrophobic core in the center of the GTPase domain that was previously shown to contribute to both basal and GPCR-accelerated nucleotide exchange in Gαi (19, 20). Structures of GPCR-bound G proteins demonstrate that GPCRs perturb the hydrophobic core directly by displacing the C-terminal α5 helix of Gαi and also inserting a hydrophobic residue from the intracellular loop 2 into the core (14–17). Thus, our findings suggest that despite binding at nonoverlapping interfaces on Gαi, GEMs and GPCRs converge on a similar mechanism for acceleration of GDP release by either directly or allosterically perturbing the intramolecular packing in the hydrophobic core of the GTPase domain of Gαi (Fig. 7). These similarities escaped detection in earlier studies employing molecular modeling (6) and NMR (45).

The presented data and model of GIV-GEM–triggered Gαi activation are in agreement with the findings of a prior study (45) where the authors investigated the same complex by NMR. The two studies converge on an almost identical set of GIV-GEM–induced increases in the dynamics of Gαi regions, including Sw-I, the β2–β3, α3–β5 and α4–β6 loops, and the NDS motif of the helical domain. In fact, the only difference between the two studies is found in the phosphate-coordinating P-loop of Gαi, where de Opakua et al. (45) report an increase in dynamics while we observe no significant difference by either HDX or MD. However, it is important to note that our experiments are conducted in the absence of excess GDP, by inherently different techniques, and, in the case of HDX, on a mutant rather than the Gαi complex with GIV; therefore, subtle variations in findings are expected. Despite this difference, the proposed dynamic model of GIV-GEM–mediated GDP release is fully consistent between the two studies, with the advance of our work being in

Mechanisms of G protein activation

Canonical — G protein α subunit — **Non-canonical**

GPCR | α5 | Hydrophobic core | GEM | Sw-II

Prior work
• GPCR signal initiated by upward movement of α5
• Direct perturbation of the hydrophobic core

GDP Release

This work
• GEM signal initiated by unique elevated Sw-II
• Allosteric perturbation of the hydrophobic core

Fig. 7. GEMs and GPCRs bind at nonoverlapping interfaces on Gαi but both perturb the hydrophobic core of the GTPase domain to stimulate GDP release. (*Left*) Structure displaying GPCR interface and subsequent Gαi dynamics that ultimately result in GDP release. (*Right*) Structure displaying GEM interface and subsequent Gαi dynamics that ultimately result in GDP release. Purple color highlights regions of Gαi that move during activation, and yellow arrows describe the direction those regions move. For clarity, only part of the GTPase domain of Gαi is shown.

providing an atomic resolution insight into the details of GIV-GEM binding and action.

Our MD simulations of the Gαi•GDP•GIV-GEM and other complexes closely recapitulate the findings from the HDX studies of the GEM-mimicking mutant W211^G.H2.7A. In the HDX studies of the mutant, several regions showed increased deuterium incorporation, with the largest increases observed in the β2 strand, α4–β6 loop, NDS loop, and α5 helix; these findings were corroborated by the MD simulations. The main difference between the HDX and MD studies was in the αD–αE loop where increased dynamics was observed in HDX but not in MD. The αD–αE loop is important for stabilizing the contacts between the Gαi GTPase and α-helical domain, thus regulating domain separation. The observed difference could be explained by insufficient sampling due to moderate length of our MD simulations (total of ~1 μs) where much longer simulations may be required to observe spontaneous domain opening (e.g., the total 42-μs Gαi-GDP as in ref. 18).

Recent studies have suggested the existence of a transition state intermediate in G protein activation (43, 46, 47). These studies utilize HDX-MS, hydroxyl radical–mediated protein footprinting MS, and computational methods to gain insight into structural changes early in the G protein activation process. These studies identified increased dynamics in the C-terminal region of the α5-helix and β2–β3 strands to be some of the earliest motions that occur during GPCR-mediated G protein activation and suggest that disruption of interactions between the α5 helix and the αN/β1 hinge and β-sheet (i.e., disruption of the hydrophobic core) may be sufficient to destabilize the nucleotide-binding pocket. In the present study, we also observe similar motions in the β2–β3 and α5 regions in both our HDX and MD studies, supporting the idea that these motions may also be part of an early event in G protein activation and GDP release triggered by GEMs. Therefore, the recent computational studies (43, 46, 47) are fully consistent with the results presented here and in the prior NMR study of GIV-GEM (45).

Because nucleotide exchange is an inherently dynamic process, our serendipitously identified His-tag linker has likely facilitated the crystallization of an otherwise unstable and transient complex, much like crystal packing for a previously crystallized accelerated exchange mutant (42) or the intentionally introduced conformation-specific nanobodies in other GEF-bound structures of G proteins (14, 48–50). Several lines of evidence support this claim. First, no crystals were obtained when the His-tag linker was removed or placed in a different position, suggesting that the linker assisted in crystallization. Second, MD simulations with and without the His-tag linker showed pronounced differences, where the presence of the linker reversed the destabilizing effects of the GIV-GEM peptide and stabilized the hydrophobic core. Finally, the similarities in Sw-I interactions between the His-tag linker and GoLoco GDIs suggested a possible mechanistic basis by which the linker counteracts the GEF action of the GIV-GEM peptide (*SI Appendix*, Fig. S3C). Importantly, despite its role in crystallization, the His-tag linker did not affect the Gαi–GEM interaction interface, as demonstrated by the comparison of our His-tag linker-containing Gαi–KB752 structure with the previously solved linker-free structure of the same complex. However, it clearly influenced the position of Sw-I, which was expected to be found in an inward-collapsed low-GDP-affinity conformation but was instead propped in a partial outward high-GDP-affinity-like conformation. This illustrates that the insights from the structure alone may be limited by its static nature, and that only the orthogonal computational, biophysical, and biochemical experiments can provide a holistic understanding of the diverse mechanisms for allosteric regulation of Gαi.

Finally, our study reveals similarities between the mechanism of action of GIV-GEM and the activation of small GTPases. It has been postulated that a common ancestor of the GTPase fold provided a structural framework that can be perturbed by the interruption of α5–α1 contacts (22). GPCRs trigger the perturbation by directly binding to α5 of their effector trimeric G protein, whereas GEFs of small GTPases typically act via binding to Sw-I and Sw-II. Our study not only supports the conserved nature of the ancestral α5–α1 activation mechanism but also suggests that similarities between monomeric GTPases and trimeric G proteins extend beyond it, because just like for small GTPases, Sw-I and Sw-II in Gαi may serve as allosteric "handles" by which the conserved exchange mechanism is accessed by modulators.

Materials and Methods

Detailed materials and methods can be found in *SI Appendix*.

Expression and Purification of His-Gαi3. The 6xHis-tagged Gαi3 constructs (6xHis-Gαi3, 6xHis-ΔN25-Gαi3, or single-point mutants thereof) were transformed into *Escherichia coli* BL21 (DE3; Invitrogen) cells. Cells were grown in 1-L flasks at 37 °C until optical density reached 0.8 to 1.0 then induced overnight at 25 °C with 1 mM isopropyl β-D-1-thiogalactopyranoside. Cells were harvested via centrifugation and lysed at 15,000 p.s.i. by a single pass through a cell disruptor (TS-Series; Constant Systems, Inc.) in running buffer (RB; 50 mM NaH₂PO₄, pH 7.4, 300 mM NaCl, and 0.5 mM EDTA) supplemented with 2× protease inhibitors (Roche Life Science) and 10 mM imidazole. Cell debris was removed by ultracentrifugation at 45,000 × g for 40 min, and the supernatant was loaded on a Ni–NTA His60 Superflow resin (Qiagen) affinity column via fast protein liquid chromatography (AKTA; GE Life Sciences). The resin was washed with RB + 60 mM imidazole and eluted with RB + 300 mM imidazole. The eluted protein was concentrated at 1,500 × g

(Amicon Ultra-15 30 molecular-weight cutoff centrifugal filter; Millipore) and subjected to size-exclusion chromatography via Superdex 200 resin (GE Healthcare) equilibrated with storage buffer (20 mM Tris·HCl, pH 7.4, 20 mM NaCl, 1 mM MgCl$_2$, and 5% glycerol). Fractions from major peak were pooled, resulting in usually ~1 to 5 mg/mL Gαi protein. Protein was then aliquoted, flash-frozen, and stored at −80 °C. Protein concentration and purity were checked throughout purification via SDS/PAGE and comparison with known amounts of BSA.

Crystallization, Data Collection, and Structure Determination. Purified 3 mg/mL 6xHis-ΔN25-Gαi3 (either freshly prepared or freeze–thawed once) was incubated overnight in storage buffer (20 mM Tris·HCl, pH 7.4, 20 mM NaCl, 1 mM MgCl$_2$, and 5% glycerol) at a 3:1 (peptide:Gαi3) molar ratio at 4 °C then concentrated to ~15 mg/mL and set on 288-well Intelli-Plate trays (Art Robbins Instruments) in 1:1, 1.5:1, and 2:1 volume ratios with mother liquor (12 to 16% PEG 3350 and 0.2 M NH$_4$Cl) at room temperature. Crystals appeared after 1 to 2 d and grew to full size in 5 to 7 d. Crystals were cryoprotected by soaking in mother liquor supplemented with 10% glycerol and flash-frozen with liquid nitrogen. X-ray diffraction data were collected at 100 K at the Lawrence Berkeley National Laboratory Advanced Light Source (8.2.2) and Stanford Synchrotron Radiation Lightsource (2, 9) at a single wavelength. All diffraction data were indexed and integrated with MOSFLM, processed with AIMLESS, and truncated with CTRUNCATE within the CCP4 suite of programs (51–53) (v.7.0.056). Phases were estimated via molecular replacement in Phaser (54) (v.2.8.1), using a previously published model of human Gαi1 (PDB ID code 1y3a, for Gαi3·GDP with KB-752) or human Gαi3 (PDB ID code 4g5r, for Gαi3·GDP with GIV-GEM) as a search model. Further details can be found in *SI Appendix*.

Molecular Modeling. Models of Gαi·GDP with (pS1674)GIV-GEM, Gαi·GDP with Daple-GEM, and Gαi·GDP with NUCB1-GEM were constructed by homology with the structure of Gαi·GDP with GIV-GEM using ICM versions 3.8-6 to 3.8-7a (Molsoft LLC).

The GEM motif peptides from (pS1674)GIV (1671-KTG-pS1674-PGSEV-VTLQQFLEESNK-1691) and Daple (1663-ASPSSEMVTLEEFLEESNR-1681) were built ab initio; the GEM motif peptide from NUCB1 (305-DTNQ-DRLVTLEEFLASTQRKEF-326) was extracted from the NMR structure of NUCB1 [PDB ID code 1snl (30)]. The backbone atoms of the peptides were confined to the crystallographic coordinates of the corresponding atoms of GIV-GEM (residues 1676-GSEVVTLQQFLEES-1689 only) via a set of harmonic distance restraints (tethers); the peptide flanks and side chains were kept unrestrained. Full-atom conformational sampling of the peptides (backbone, side chains, and positional variables) and the surrounding side chains of Gαi was performed using 5 × 10^6 steps of biased probability Monte Carlo optimization (55) as implemented in ICM, with the repulsive part of the van der Waals potential capped at 20 kJ/mol. The top scoring pose of each peptide was selected for analysis.

MANT-GTPγS Incorporation Assays. MANT-GTPγS incorporation into Gαi3 was quantified, either by FRET (excitation = 280; emission = 440) or by direct MANT excitation (excitation = 350; emission = 440) using a microplate fluorescence reader (Tecan Spark 20M). Fluorescence was measured every 30 s starting immediately after injection of MANT-GTPγS. Raw fluorescence was plotted over time and observed rates (k$_{obs}$) were determined by fitting a one-phase association curve to the data (GraphPad Prism v.7). Further details can be found in *SI Appendix*.

HDX-MS. HDX-MS measurements were made using a Synapt G2Si system (Waters Corporation). Deuterium exchange reactions were carried out by a Leap HDX PAL autosampler (Leap Technologies). Deuterated buffer was prepared by lyophilizing 10 mL of 20 mM Tris·HCl, pH 7.4, 20 mM NaCl, 5 μM GDP, and 5% glycerol and resuspending it in 10 mL 99.96% D$_2$O immediately before use. Each deuterium exchange time point (0 min, 1 min, 2.5 min, 5 min) was measured in triplicate. For each measurement, 5 μL of 100 μM 6xHis-Gαi3 protein in storage buffer (20 mM Tris·HCl, pH 7.4, 20 mM NaCl, 1 mM MgCl$_2$, and 5% glycerol) was mixed with 55 μL of D$_2$O buffer at 25 °C. Deuterium exchange was quenched by combining 50 μL of the deuterated sample with 50 μL of 0.1% formic acid and 3 M guanidinum-HCl for 1 min at 1 °C. The quenched sample was then injected in a 50-μL sample loop and digested by an inline pepsin column (Pierce, Inc.) at 15 °C. The resulting peptides were captured on a BEH C18 Vanguard precolumn, separated by analytical chromatography (Acquity UPLC BEH C18, 1.7 μm, 1.0 × 50 mm; Waters Corporation) using 7 το 85% acetonitrile in 0.1% formic acid over 7.5 min and analyzed in a Waters Synapt G2Si quadrupole time-of-flight mass spectrometer following electrospray injection. Data were collected in

Mobility, ESI+ mode, mass acquisition range of 200 to 2,000 (*m/z*), scan time 0.4 s. Continuous lock mass correction was performed using infusion of leu-enkephalin (*m/z* = 556.277) every 30 s (mass accuracy of 1 ppm for calibration standard). For peptide identification, data were instead collected in MS E (mobility ESI+) mode. Peptides masses were identified following triplicate analysis of 10 μM Gαi3 and were analyzed using PLGS 2.5 (Waters Corporation). Further details can be found in *SI Appendix*.

MD Simulations. MD simulations were performed for three complexes: Gαi·GDP, Gαi·GDP with GIV-GEM, and Gαi·GDP with GIV-GEM and His-tag linker (amino acid residues GLVPRGS from the linker of the crystallographic neighbor molecule), using the AMBER package (v. 16) as described in *SI Appendix*.

MD Trajectory Analysis. MD simulation analyses were performed in ICM v.3.8-7a (Molsoft LLC), unless otherwise stated. Replicate simulations of a single condition were concatenated together for analysis.

For RMSF analysis, MD frames from each condition were superimposed by the backbone (C, N, O, and Cα atoms), using cpptraj, within the AMBER package (56) (v.16). The coordinates of the center of mass of each Gαi residue *j* at frame *f*, $r_f(j) = \langle x_f(j), y_f(j), z_f(j) \rangle$, were given by

$$r_f(j) = \frac{\sum_{a \in A_j} m(a) \times r(a)}{\sum_{a \in A_j} m(a)},$$

where A_j is the set of all nonhydrogen atoms in residue *j*, $m(a)$ is the atomic weight of atom *a*, and $r(a) = \langle x(a), y(a), z(a) \rangle$ is the vector of Cartesian coordinates of atom *a*. The mean coordinates of residue *j* over all *F* frames of the trajectory were calculated as $\bar{r}(j) = \frac{1}{F} \sum_{f=1}^{F} r_f(j)$, and the RMSF of residue *j* as

$$RMSF_j = \sqrt{\frac{1}{F} \sum_{f=1}^{F} |r_f(j) - \bar{r}(j)|^2},$$

where || denotes the length of the vector in Cartesian coordinates. Differences in residue RMSF between the MD conditions were mapped onto the crystal structure and visualized.

To trace intramolecular motions in Gαi induced by GIV-GEM, Euclidean distances between centers of mass of amino acid residue pairs, or between residues and GDP (50,721 pairs total), were calculated for each frame of the simulation. Residue pairs were filtered to retain only 1658 pairs that satisfied the following criteria: 1) they were at least two residues apart in the sequence; 2) they were separated by less than 12 Å in at least one MD frame; 3) their distances displayed less than 75% overlap in frequency distribution between the Gαi·GDP and Gαi·GDP+GIV-GEM simulations; and 4) they did not involve Sw-II residues (residues 202$^{G.s3h2.1}$ to 218$^{G.h2s4.4}$). To calculate the overlap between the distance frequency distributions, the distance range was broken into *b* 0.2-Å intervals and the binned relative frequencies of the center of mass distance were computed for each pair of residues *i, j* over the course of the Gαi·GDP trajectory:

$$\left\langle p_1^{GDP}(i,j), p_2^{GDP}(i,j), \ldots, p_b^{GDP}(i,j) \right\rangle, \sum_{k=1}^{b} p_k^{GDP}(i,j) = 1$$

and the same was done for the Gαi·GDP+GIV-GEM trajectory, giving $p_k^{GIV}(i,j), k \in \{1, \ldots, b\}$. The overlap was given by $\sum_{k=1}^{b} \min(p_k^{GDP}(i,j), p_k^{GIV}(i,j))$. The 1,658 nontrivial residue pairs were subjected to PCA to identify those pairs whose changing distances contribute the most to the dominant modes of motion upon GIV-GEM binding, in an unbiased manner. Only the first PC was analyzed because it correctly discriminated the simulation conditions (*SI Appendix*, Fig. S8B). Residue pairs assigned with the largest weights and associated with the first PC were mapped onto the crystal structure for visualization.

Statistical Analysis. Each experiment presented in the figures is representative of at least three independent repeats (with at least two technical repeats for each condition within each repeat). Statistical significance between the differences of means was calculated using multiple comparisons in one-way nonparametric ANOVA. All statistics and graphical data presented were prepared using GraphPad Prism v.7. Histograms of MD simulation data were generated in R v.3.4.4. All error bars are SD.

1. A. G. Gilman, G proteins: Transducers of receptor-generated signals. *Annu. Rev. Biochem.* **56**, 615–649 (1987).
2. A. J. Morris, C. C. Malbon, Physiological regulation of G protein-linked signaling. *Physiol. Rev.* **79**, 1373–1430 (1999).
3. D. P. Siderovski, F. S. Willard, The GAPs, GEFs, and GDIs of heterotrimeric G-protein alpha subunits. *Int. J. Biol. Sci.* **1**, 51–66 (2005).
4. N. Aznar, N. Kalogriopoulos, K. K. Midde, P. Ghosh, Heterotrimeric G protein signaling via GIV/Girdin: Breaking the rules of engagement, space, and time. *BioEssays* **38**, 379–393 (2016).
5. P. Ghosh, P. Rangamani, I. Kufareva, The GAPs, GEFs, GDIs and...now, GEMs: New kids on the heterotrimeric G protein signaling block. *Cell Cycle* **16**, 607–612 (2017).
6. M. Garcia-Marcos, P. Ghosh, M. G. Farquhar, GIV is a nonreceptor GEF for G alpha i with a unique motif that regulates Akt signaling. *Proc. Natl. Acad. Sci. U.S.A.* **106**, 3178–3183 (2009).
7. V. Gupta et al., GIV/Girdin activates Gαi and inhibits Gαs via the same motif. *Proc. Natl. Acad. Sci. U.S.A.* **113**, E5721–E5730 (2016).
8. C. A. Johnston et al., Structure of Galpha(i1) bound to a GDP-selective peptide provides insight into guanine nucleotide exchange. *Structure* **13**, 1069–1080 (2005).
9. G. S. Ma et al., Therapeutic effects of cell-permeant peptides that activate G proteins downstream of growth factors. *Proc. Natl. Acad. Sci. U.S.A.* **112**, E2602–E2610 (2015).
10. K. K. Midde et al., Multimodular biosensors reveal a novel platform for activation of G proteins by growth factor receptors. *Proc. Natl. Acad. Sci. U.S.A.* **112**, E937–E946 (2015).
11. K. Parag-Sharma et al., Membrane recruitment of the non-receptor protein GIV/girdin (Gα-interacting, vesicle-associated protein/girdin) is sufficient for activating heterotrimeric G protein signaling. *J. Biol. Chem.* **291**, 27098–27111 (2016).
12. I. Lopez-Sanchez et al., GIV/Girdin is a central hub for profibrogenic signalling networks during liver fibrosis. *Nat. Commun.* **5**, 4451 (2014).
13. P. Ghosh, Heterotrimeric G proteins as emerging targets for network based therapy in cancer: End of a long futile campaign striking heads of a Hydra. *Aging (Albany N.Y.)* **7**, 469–474 (2015).
14. S. G. Rasmussen et al., Crystal structure of the β2 adrenergic receptor-Gs protein complex. *Nature* **477**, 549–555 (2011).
15. A. Koehl et al., Structure of the μ-opioid receptor-Gᵢ protein complex. *Nature* **558**, 547–552 (2018).
16. B. Carpenter, R. Nehmé, T. Warne, A. G. Leslie, C. G. Tate, Structure of the adenosine A(2A) receptor bound to an engineered G protein. *Nature* **536**, 104–107 (2016).
17. C. J. Draper-Joyce et al., Structure of the adenosine-bound human adenosine A₁ receptor-Gᵢ complex. *Nature* **558**, 559–563 (2018).
18. R. O. Dror et al., SIGNAL TRANSDUCTION. Structural basis for nucleotide exchange in heterotrimeric G proteins. *Science* **348**, 1361–1365 (2015).
19. A. I. Kaya et al., A conserved phenylalanine as a relay between the α5 helix and the GDP binding region of heterotrimeric Gi protein α subunit. *J. Biol. Chem.* **289**, 24475–24487 (2014).
20. A. I. Kaya et al., A conserved hydrophobic core in Gαi1 regulates G protein activation and release from activated receptor. *J. Biol. Chem.* **291**, 19674–19686 (2016).
21. M. Garcia-Marcos, P. Ghosh, M. G. Farquhar, GIV/Girdin transmits signals from multiple receptors by triggering trimeric G protein activation. *J. Biol. Chem.* **290**, 6697–6704 (2015).
22. T. Flock et al., Universal allosteric mechanism for Gα activation by GPCRs. *Nature* **524**, 173–179 (2015).
23. S. R. Sprang, Invited review: Activation of G proteins by GTP and the mechanism of Gα-catalyzed GTP hydrolysis. *Biopolymers* **105**, 449–462 (2016).
24. M. Garcia-Marcos, J. Ear, M. G. Farquhar, P. Ghosh, A GDI (AGS3) and a GEF (GIV) regulate autophagy by balancing G protein activity and growth factor signals. *Mol. Biol. Cell* **22**, 673–686 (2011).
25. D. Bhandari et al., Cyclin-dependent kinase 5 activates guanine nucleotide exchange factor GIV/Girdin to orchestrate migration-proliferation dichotomy. *Proc. Natl. Acad. Sci. U.S.A.* **112**, E4874–E4883 (2015).
26. I. López-Sánchez et al., Protein kinase C-theta (PKCθ) phosphorylates and inhibits the guanine exchange factor, GIV/Girdin. *Proc. Natl. Acad. Sci. U.S.A.* **110**, 5510–5515 (2013).
27. M. Garcia-Marcos, P. Ghosh, J. Ear, M. G. Farquhar, A structural determinant that renders G alpha(i) sensitive to activation by GIV/girdin is required to promote cell migration. *J. Biol. Chem.* **285**, 12765–12777 (2010).
28. N. Aznar et al., Daple is a novel non-receptor GEF required for trimeric G protein activation in Wnt signaling. *eLife* **4**, e07091 (2015).
29. M. Garcia-Marcos, P. S. Kietrsunthorn, H. Wang, P. Ghosh, M. G. Farquhar, G Protein binding sites on Calnuc (nucleobindin 1) and NUCB2 (nucleobindin 2) define a new class of G(alpha)i-regulatory motifs. *J. Biol. Chem.* **286**, 28138–28149 (2011).
30. E. de Alba, N. Tjandra, Structural studies on the Ca2+-binding domain of human nucleobindin (calnuc). *Biochemistry* **43**, 10039–10049 (2004).
31. R. J. Kimple, M. E. Kimple, L. Betts, J. Sondek, D. P. Siderovski, Structural determinants for GoLoco-induced inhibition of nucleotide release by Galpha subunits. *Nature* **416**, 878–881 (2002).
32. A. S. Raw, D. E. Coleman, A. G. Gilman, S. R. Sprang, Structural and biochemical characterization of the GTPgammaS-, GDP.Pi-, and GDP-bound forms of a GTPase-deficient Gly42–> Val mutant of Gialpha1. *Biochemistry* **36**, 15660–15669 (1997).
33. A. E. Remmers, Detection and quantitation of heterotrimeric G proteins by fluorescence resonance energy transfer. *Anal. Biochem.* **257**, 89–94 (1998).
34. D. Goricanec et al., Conformational dynamics of a G-protein α subunit is tightly regulated by nucleotide binding. *Proc. Natl. Acad. Sci. U.S.A.* **113**, E3629–E3638 (2016).
35. K. M. Ferguson, T. Higashijima, M. D. Smigel, A. G. Gilman, The influence of bound GDP on the kinetics of guanine nucleotide binding to G proteins. *J. Biol. Chem.* **261**, 7393–7399 (1986).
36. M. A. Wall et al., The structure of the G protein heterotrimer Gi alpha 1 beta 1 gamma 2. *Cell* **83**, 1047–1058 (1995).
37. T. E. Wales, J. R. Engen, Hydrogen exchange mass spectrometry for the analysis of protein dynamics. *Mass Spectrom. Rev.* **25**, 158–170 (2006).
38. R. B. Peacock, J. R. Davis, P. R. L. Markwick, E. A. Komives, Dynamic consequences of mutation of tryptophan 215 in thrombin. *Biochemistry* **57**, 2694–2703 (2018).
39. R. Kant, B. Zeng, C. J. Thomas, B. Bothner, S. R. Sprang, Ric-8A, a G protein chaperone with nucleotide exchange activity induces long-range secondary structure changes in Gα. *eLife* **5**, e19238 (2016).
40. G. S. Anand, C. A. Hughes, J. M. Jones, S. S. Taylor, E. A. Komives, Amide H/2H exchange reveals communication between the cAMP and catalytic subunit-binding sites in the R(I)alpha subunit of protein kinase A. *J. Mol. Biol.* **323**, 377–386 (2002).
41. D. E. Coleman, S. R. Sprang, Crystal structures of the G protein Gi alpha 1 complexed with GDP and Mg2+: A crystallographic titration experiment. *Biochemistry* **37**, 14376–14385 (1998).
42. N. Kapoor, S. T. Menon, R. Chauhan, P. Sachdev, T. P. Sakmar, Structural evidence for a sequential release mechanism for activation of heterotrimeric G proteins. *J. Mol. Biol.* **393**, 882–897 (2009).
43. X. Sun, S. Singh, K. J. Blumer, G. R. Bowman, Simulation of spontaneous G protein activation reveals a new intermediate driving GDP unbinding. *eLife* **7**, e38465 (2018).
44. D. Sun et al., Probing Gαi1 protein activation at single-amino acid resolution. *Nat. Struct. Mol. Biol.* **22**, 686–694 (2015).
45. A. I. de Opakua et al., Molecular mechanism of Gαi activation by non-GPCR proteins with a Gα-Binding and Activating motif. *Nat. Commun.* **8**, 15163 (2017).
46. Y. Du et al., Assembly of a GPCR-G protein complex. *Cell* **177**, 1232–1242.e11 (2019).
47. X. Liu et al., Structural insights into the process of GPCR-G protein complex formation. *Cell* **177**, 1243–1251.e12 (2019).
48. T. Che et al., Structure of the nanobody-stabilized active state of the kappa opioid receptor. *Cell* **172**, 55–67.e15 (2018).
49. W. Huang et al., Structural insights into μ-opioid receptor activation. *Nature* **524**, 315–321 (2015).
50. A. C. Kruse et al., Activation and allosteric modulation of a muscarinic acetylcholine receptor. *Nature* **504**, 101–106 (2013).
51. T. G. Battye, L. Kontogiannis, O. Johnson, H. R. Powell, A. G. Leslie, iMOSFLM: A new graphical interface for diffraction-image processing with MOSFLM. *Acta Crystallogr. D Biol. Crystallogr.* **67**, 271–281 (2011).
52. P. Evans, Scaling and assessment of data quality. *Acta Crystallogr. D Biol. Crystallogr.* **62**, 72–82 (2006).
53. M. D. Winn et al., Overview of the CCP4 suite and current developments. *Acta Crystallogr. D Biol. Crystallogr.* **67**, 235–242 (2011).
54. A. J. McCoy et al., Phaser crystallographic software. *J. Appl. Cryst.* **40**, 658–674 (2007).
55. R. Abagyan, M. Totrov, Biased probability Monte Carlo conformational searches and electrostatic calculations for peptides and proteins. *J. Mol. Biol.* **235**, 983–1002 (1994).
56. D. R. Roe, T. E. Cheatham, 3rd, PTRAJ and CPPTRAJ: Software for processing and analysis of molecular dynamics trajectory data. *J. Chem. Theory Comput.* **9**, 3084–3095 (2013).
57. I. Kufareva, M. Rueda, V. Katritch, R. C. Stevens, R. Abagyan; GPCR Dock 2010 participants, Status of GPCR modeling and docking as reflected by community-wide GPCR Dock 2010 assessment. *Structure* **19**, 1108–1126 (2011).

BIOPHYSICS AND COMPUTATIONAL BIOLOGY